

the plant journal**Subdiffraction-resolution live-cell imaging for visualizing thylakoid membranes**

Journal:	<i>The Plant Journal</i>
Manuscript ID	TPJ-00552-2018.R1
Manuscript Type:	Technical Advance
Date Submitted by the Author:	n/a
Complete List of Authors:	Iwai, Masakazu; Lawrence Berkeley National Laboratory, Molecular Biophysics & Integrated Bioimaging Division; University of California Berkeley, Department of Plant and Microbial Biology Roth, Melissa; University of California Berkeley, Department of Plant and Microbial Biology Niyogi, Krishna; University of California, Department of Plant & Microbial Biology; Lawrence Berkeley National Laboratory, Molecular Biophysics & Integrated Bioimaging Division
Key Words:	structured illumination microscopy, live-cell imaging, thylakoid structure, Arabidopsis thaliana, Chlamydomonas reinhardtii

SCHOLARONE™
Manuscripts

1
2
3 TECHNICAL ADVANCE
4
5

6 **Subdiffraction-resolution live-cell imaging for visualizing**
7 **thylakoid membranes**
8
9

10
11
12 **Masakazu Iwai^{1,2,*}, Melissa S. Roth² and Krishna K. Niyogi^{1,2,*}**
13
14

15
16 *¹Molecular Biophysics and Integrated Bioimaging Division, Lawrence Berkeley National*
17 *Laboratory, Berkeley, CA 94720, USA, and*

18
19 *²Department of Plant and Microbial Biology, Howard Hughes Medical Institute, University of*
20 *California, Berkeley, CA 94720-3102, USA.*
21
22

23
24 For correspondence (email miwai@berkeley.edu or niyogi@berkeley.edu).
25
26

27 Keywords: structured illumination microscopy, live-cell imaging, thylakoid structure, *Arabidopsis*
28 *thaliana*, *Chlamydomonas reinhardtii*
29
30
31
32
33
34
35
36
37
38
39
40
41
42
43
44
45
46
47
48
49
50
51
52
53
54
55
56
57
58
59
60

SUMMARY

The chloroplast is the chlorophyll-containing organelle that produces energy through photosynthesis. Within the chloroplast is an intricate network of thylakoid membranes containing photosynthetic membrane proteins that mediate electron transport and generate chemical energy. Historically, electron microscopy has been a powerful tool to visualize the macromolecular structure and organization of thylakoid membranes. However, understanding thylakoid membrane dynamics remains elusive because electron microscopy requires fixation and sectioning. To improve knowledge of thylakoid membrane dynamics, we need to overcome at least two issues: 1) the live-cell imaging conditions to visualize active processes *in vivo*; and 2) the spatial resolution to differentiate thylakoid membrane characteristics. Here, we utilize three-dimensional structured illumination microscopy (3D-SIM) to explore the optimal imaging conditions to investigate the dynamics of thylakoid membranes in live cells of plants and algae. We show that 3D-SIM is capable of examining broad characteristics of thylakoid structures in chloroplasts of the vascular plant *Arabidopsis thaliana* and distinguishing the structural differences between wild-type and mutant strains. Using 3D-SIM, we also visualize thylakoid organization in whole cells of the green alga *Chlamydomonas reinhardtii*. These data reveal that high light intensity changes thylakoid membrane structure in *C. reinhardtii*. Moreover, we observed the green alga *Chromochloris zofingiensis* and the moss *Physcomitrella patens* to show the applicability of 3D-SIM. This study demonstrates that 3D-SIM is a promising approach to study the dynamics of thylakoid membranes in photoautotrophic organisms during photoacclimation processes.

Significance Statement

A key to understanding dynamic mechanisms of photosynthesis and photoprotection in chloroplast thylakoid membranes is to examine the processes *in vivo*. However, technical limitations in spatial resolution have prevented *in vivo* observations of thylakoid membrane dynamics. Here, we use live-cell three-dimensional structured illumination microscopy (3D-SIM) to investigate such dynamic processes occurring within chloroplasts at unprecedented spatiotemporal scales.

INTRODUCTION

Light energy is essential for photosynthesis, and environmental fluctuations in light conditions affect biomass and growth of green algae and plants. Regulation of photosynthetic light harvesting is a key component to maintain efficient photosynthesis under changing light conditions (Horton *et al.* 1996, Niyogi 1999, Ruban 2016, Wobbe *et al.* 2016). Light energy captured by light-harvesting complex (LHC) proteins is transferred to two photosystems (PSI and PSII) where their reaction centers undergo charge separation to initiate electron transfer (Nelson 2011). The different macrostructures comprised of photosystems and their associated LHC proteins affect the rate of excitation energy transfer (Caffarri *et al.* 2011, Valkunas *et al.* 2011). Under fluctuating light conditions, the rearrangements of LHC proteins and their connections with photosystems occur to fine-tune the photochemical reactions (Betterle *et al.* 2009, Wientjes *et al.* 2013). Such rearrangements cause changes in the macroorganization of thylakoid membrane structures (Johnson *et al.* 2011, Goral *et al.* 2012, Kouril *et al.* 2013, Wood *et al.* 2018). Multiple different transcriptional and post-translational levels of regulation are involved in such photoacclimation mechanisms (Rochaix 2014, Erickson *et al.* 2015). However, how the dynamic reorganization of the macrostructure involving photosystems and their LHC proteins is regulated in thylakoid membranes is unknown due to the technical limitations required to visualize such intraorganellar membranes *in vivo*.

Recent advancements of cryo-electron tomography (cryo-ET) (Beck and Baumeister 2016) have enabled *in vivo* volumetric visualization of thylakoid membranes. The reconstructed three-dimensional (3D) thylakoid structures of vascular plants from cryo-ET, which are obtained by serial sections of stained chloroplasts that are cryo-immobilized and dehydrated by freeze substitution, reveal unique branching structure connecting grana (stacked membrane regions) and stroma lamellae (non-stacked membrane regions) (Shimoni *et al.* 2005, Austin and Staehelin 2011). Under increased light conditions, cryo-ET of unstained *Arabidopsis thaliana* leaves shows light-induced expansion in the lumenal space of grana suggesting diffusion in the lumen is increased under light conditions (Kirchhoff *et al.* 2011). Recently, the combination of cryo-ET and cryo-focused ion beam to obtain thin cryo-sections has been successful to generate the first 3D thylakoid structures of the unicellular green alga *Chlamydomonas reinhardtii* (Engel *et al.* 2015). This reconstruction details the membrane characteristics in the cup-shaped chloroplast including the convergent membrane tip pointing toward the chloroplast envelope and the tubular membranes around and inside the pyrenoid (Engel, *et al.* 2015). Although electron microscopy (EM) provides spatial resolution sufficient to distinguish thylakoid membranes and lumenal space, major drawbacks are that the samples need to be fixed and sectioned, which

1
2
3 makes it impossible to observe dynamic behaviors occurring within a whole chloroplast in its
4 native state.
5

6 Confocal laser scanning microscopy provides the ability to observe dynamic and native
7 behaviors in live cells, but compromises higher spatial resolution. Because thylakoid membranes
8 contain chlorophyll (Chl)-binding proteins, it is simple to observe Chl fluorescence in thylakoid
9 membranes without staining or expressing transgenic fluorescent proteins. However, it is difficult
10 to obtain clear images of thylakoid structure within chloroplasts with conventional microscopes
11 because of the high abundance of Chl pigments in thylakoid membranes. Thylakoid membranes
12 form intricate networks of grana and stroma lamellae structures that are about 5–10 μm in size. It
13 is possible to visualize thylakoid membranes in the moss *Physcomitrella patens* with increased
14 spatial resolution using 3D image deconvolution processing and determining photon-emitting
15 positions through reverse calculation of the convolved point spread function (Iwai *et al.* 2014,
16 Iwai *et al.* 2016). In this study, we applied 3D structured illumination microscopy (3D-SIM) to
17 characterize thylakoid membranes in chloroplasts of *A. thaliana* and *C. reinhardtii* at
18 subdiffraction resolution. Structured illumination microscopy (SIM) provides the ability to achieve
19 lateral resolution beyond the diffraction limit by the excitation of laterally defined patterned light
20 ("structured illumination") in a widefield microscope. Applying 3D imaging by obtaining the axial
21 information enhances the resolution to 100–130 nm in lateral dimensions and 280–350 nm in the
22 axial dimension (Gustafsson *et al.* 2008). Our results suggest that 3D-SIM is capable of
23 differentiating overall thylakoid characteristics caused by different light growth conditions and in
24 different mutant lines. This study provides proof of principle that 3D-SIM can be exploited to
25 understand dynamic behaviors of thylakoid membranes in live cells.
26
27
28
29
30
31
32
33
34
35
36
37
38

39 RESULTS

40 Differentiating *in vivo* thylakoid characteristics in whole *A. thaliana* chloroplasts using 41 3D-SIM. 42 43

44 In this study, we used a commercially available Carl Zeiss Elyra PS.1 SIM (see Experimental
45 Procedures for details). Chl fluorescence can be used to visualize thylakoid structures because
46 Chl-binding membrane proteins are abundant proteins distributed throughout thylakoid
47 membranes. We observed chloroplasts in the mesophyll tissues of the *A. thaliana* wild-type (WT)
48 leaves. Because of the numerous Chl pigments in thylakoid membranes, Chl fluorescence
49 intensity in the widefield images was too high to distinguish actual signals from background noise
50 (Figure 1a). This common problem prevents visualization of fine thylakoid membrane structures.
51 To obtain subdiffraction resolution of a fluorescence image, 3D-SIM requires acquisition of
52
53
54
55
56
57
58
59
60

1
2
3 multiple images with the excitation of structured illumination with 3–5 phase shifts at 3–5 different
4 angles (Demmerle *et al.* 2017). The final image is reconstructed through post-processing with
5 mathematical algorithms. In the reconstructed 3D-SIM image, each granum within the
6 chloroplast was clearly visible by Chl fluorescence (Figure 1b).
7
8

9 To examine if 3D-SIM was capable of differentiating structural differences in thylakoids,
10 we compared *in vivo* grana size of *A. thaliana* WT and specific mutant lines. *In vivo* grana size
11 was determined by measuring the full-width at the half maximum (FWHM; the distance between
12 points on the Gaussian distribution where the value is half of its peak value) of grana Chl
13 fluorescence from reconstructed 3D-SIM images with subdiffraction resolution. We used mutant
14 lines *stn7 stn8* and *tap38*, which possess larger and smaller grana size observed by EM,
15 respectively (Fristedt *et al.* 2009, Armbruster *et al.* 2013). For 8 chloroplasts in the mesophyll
16 tissues of WT and both mutants, we measured FWHM of all clearly defined grana in each
17 chloroplast (Figure 1b-d). WT had grana FWHM of 321 ± 38 nm (Figure 1g; $n = 300$ from 8
18 chloroplasts). By comparison, the grana FWHM of *stn7 stn8* mutant was 620 ± 99 nm (Figure 1h;
19 $n = 124$ from 8 chloroplasts), which was roughly twice as large as *tap38* mutant at 299 ± 43 nm
20 (Figure 1i; $n = 251$ from 8 chloroplasts). Such a large difference was previously observed by EM
21 (Armbruster, *et al.* 2013). We also observed that the number of grana present within *stn7 stn8*
22 was about half that of *tap38* mutant, which suggests that the total volume of thylakoid
23 membranes may be equal between the two mutants. While these results showed minimal
24 variation of grana size within an individual chloroplast and among chloroplasts, this technique
25 provides the ability to quantify these characteristics.
26
27
28
29
30
31
32
33
34
35

36 To test whether 3D-SIM can differentiate thylakoid structural characteristics caused by
37 different light conditions, we observed grana from *A. thaliana* WT acclimated to far-red (FR) or
38 blue (BL) light for 2 h (Figure 1e,f), the conditions known to induce dephosphorylation or
39 phosphorylation of LHC proteins of PSII (LHCII) by the TAP38/PPH1 phosphatase (Pribil *et al.*
40 2010, Shapiguzov *et al.* 2010) or STN7 kinase (Bellafiore *et al.* 2005), respectively. These results
41 indicated that the FWHM of FR- and BL-acclimated grana was 370 ± 50 nm (Figure 1j; $n = 149$
42 from 8 chloroplasts) and 304 ± 38 nm (Figure 1k; $n = 172$ from 8 chloroplasts), respectively. The
43 BL-acclimated chloroplasts showed similar average FWHM to the *tap38* mutant, because BL
44 acclimation and *tap38* are both known to promote LHCII phosphorylation (Haldrup *et al.* 2001,
45 Pribil, *et al.* 2010, Shapiguzov, *et al.* 2010). In contrast, the grana of FR-acclimated chloroplasts
46 were not as large as in the *stn7 stn8* mutant, most likely because FR light does not have a major
47 effect on the dephosphorylation of PSII core proteins, which involves the STN8 kinase, whereas
48 the *stn7 stn8* mutant shows almost complete dephosphorylation of both LHCII and PSII core
49
50
51
52
53
54
55
56
57
58
59
60

1
2
3 proteins (Bonardi *et al.* 2005). Although there were variations among different chloroplasts, the
4 difference between BL- and FR-acclimated grana size observed by 3D-SIM was statistically
5 significant (Student's t-test, $P < 0.0001$).
6
7

8 In mesophyll chloroplasts of *A. thaliana* leaves, the grana stacks are usually oriented
9 perpendicular to the leaf surface (Figure 1). While the side-view of thylakoid structures is rarely
10 observable *in vivo*, it is possible to image this view by 3D-SIM with isolated intact chloroplasts. To
11 visualize the side-view of chloroplasts by 3D-SIM, we resuspended isolated intact chloroplasts in
12 low-melting point agarose medium, which embedded and immobilized chloroplasts in random
13 orientation. The reconstructed 3D-SIM images show the side-view of whole isolated chloroplasts,
14 in which the layered membrane structures of the grana were visible (Figure 2a-c). This
15 orientation is similar to what is usually observed in chemically or cryogenically fixed and
16 sectioned leaves by EM. However, because light microscopy is capable of optical sectioning
17 through samples, it is possible to analyze the membrane structures through the whole
18 chloroplast in a nondestructive way with 3D-SIM (Figures S1–3). From reconstructed 3D-SIM
19 images, we measured the thickness of each layer of thylakoid membranes (Figure 2d,e). The
20 FWHM of each layer was similar among WT and the two mutants—WT: 131 ± 27 nm ($n = 27$ from
21 5 chloroplasts); *stn7 stn8*: 133 ± 23 nm ($n = 30$ from 5 chloroplasts); and *tap38*: 119 ± 24 nm ($n =$
22 29 from 5 chloroplasts). The thinnest FWHM observed was 85 nm. A previous cryo-EM study
23 (Kirchhoff, *et al.* 2011) found that the stacking repeat distance (*i.e.*, the thickness of two thylakoid
24 membrane bilayers, the lumen, and a stromal gap between appressed membrane bilayers) of *A.*
25 *thaliana* grana thylakoids is 15.7–16.3 nm under normal conditions. Using the reported stacking
26 repeat distance, the thinnest layer we observed (85 nm) could contain at most 5 grana discs.
27 Because of this limitation in spatial resolution, it is not practical to quantify the thickness of grana
28 stacks, although the overall side-view of chloroplasts showed thylakoid membrane structures
29 that appeared to include grana and stroma lamellae (Figure 2a-c).
30
31
32
33
34
35
36
37
38
39
40
41
42

43 Comparing the overall side-view of chloroplasts from WT, *stn7 stn8* mutant, and *tap38*
44 mutant showed differences in apparent membrane lengths (from one edge to the other edge of a
45 clearly defined membrane) (Figure 2a–c). We measured the length of membranes by ImageJ
46 software, and these results indicated that the *stn7 stn8* mutant had the longest membranes
47 (Figure 2f). While there was minimal variation among chloroplasts of the same genotype, this
48 technique enables quantification of the differences in thylakoid membrane length between
49 genotypes (Figure 2f). Although the differences appear small, the membrane length of *tap38*
50 chloroplasts is statistically shorter than those in WT (Figure 2f; Student's t-test, $P < 0.001$). These
51 results are similar to the grana diameter quantifications in the *stn7 stn8* and the *tap38*
52
53
54
55
56
57
58
59
60

1
2
3 chloroplasts (Figure 1c, e), suggesting that 3D-SIM is capable of visualizing the traditional
4 side-view of chloroplasts in a nondestructive way that maintains the native conditions observed
5 *in vivo*.
6
7

9 **Visualizing *in vivo* thylakoid membrane characteristics and structural dynamics in whole** 10 **cells of *C. reinhardtii* using 3D-SIM.**

11
12 To assess 3D-SIM capabilities with algae, we imaged thylakoid membranes of the model
13 unicellular green alga *C. reinhardtii*. To minimize cellular movements caused by flagellar activity,
14 we embedded live cells of *C. reinhardtii* in low-melting point agarose media (see Experimental
15 Procedures for details). Similar to what we observed with *A. thaliana* chloroplasts, Chl
16 fluorescence intensity of widefield images was too high to distinguish the thylakoid structures in
17 the cells (Figure 3a,c). After reconstructing 3D-SIM images, the structures of thylakoid
18 membranes were revealed (Figure 3b,d, Figure S4). Our 3D-SIM reconstructions confirm broadly
19 appressed thylakoid membrane regions in *C. reinhardtii* chloroplasts as reported in the literature,
20 which contrasts with the distinct grana structure observed in vascular plants (as shown in Figure
21 1). Optical sectioning showed that membrane structures extend into the pyrenoid (Figure 3e,
22 arrows), verifying previous observations by cryo-ET (Engel, *et al.* 2015) and confocal microscopy
23 (Mackinder *et al.* 2017). We also observed the thylakoid tip convergence region (Figure 3f), as
24 described by cryo-ET images (Engel, *et al.* 2015). We also measured the thickness of each
25 membrane region observed by reconstructed 3D-SIM images. The average thickness of each
26 layer was 124.0 ± 20.3 nm ($n = 38$) (Figure 3f,g), but the thinnest membrane region was 74.9 nm.
27 The stacking repeat distance of *C. reinhardtii* thylakoids, as determined by cryo-ET, is 22.4 ± 1.3
28 nm (Engel, *et al.* 2015). Using the reported stacking repeat distance, it is likely that the thinnest
29 layer we observed (Figure 3f,g) contained three or fewer layers of stacked thylakoids.
30
31
32
33
34
35
36
37
38
39
40

41 Optical sectioning through the whole chloroplast enabled us to investigate unique
42 thylakoid membrane structures in the cup-shaped chloroplast in *C. reinhardtii* (Figure 3). We
43 used similar methods as our 3D-SIM analyses on *A. thaliana* (as shown in Figure 2). We
44 reconstructed 3D-SIM images from *C. reinhardtii* cells grown photoautotrophically and
45 heterotrophically under dim light conditions (DL; $\sim 5 \mu\text{mol photons m}^{-2} \text{s}^{-1}$). We observed a wide
46 variety of thylakoid membrane structures and overall appearances in different cells from the
47 same condition (Figure 4a,b). By adjusting the focal plane to near the cell surface, we could
48 observe the membrane surface patterns, which are usually difficult to obtain by EM observation.
49 The reconstructed 3D-SIM images revealed randomly shaped membrane surface patterns,
50 which showed continuous membrane regions with occasional empty spaces (Figure 4a,b). It is
51
52
53
54
55
56
57
58
59
60

1
2
3 apparent that the size, shape, and location of empty spaces on membranes are not uniformly
4 arranged. Such random patterns of empty spaces make the membrane organization observed at
5 the central focal planes look different in each cell. Surprisingly, we did not observe apparent
6 differences in membrane structures between photoautotrophically and heterotrophically grown
7 cells under DL despite reported differences in photosynthesis and light harvesting (Heifetz *et al.*
8 2000).
9

10
11 Intriguingly, 3D-SIM observations revealed that many *C. reinhardtii* cells grown
12 photoautotrophically under low light conditions (LL; $\sim 50 \mu\text{mol photons m}^{-2} \text{ s}^{-1}$) had patchy
13 membrane surface patterns (Figure 4c, slice numbers 1–10). Moreover, after one day of growing
14 under high light conditions (HL; $\sim 350 \mu\text{mol photons m}^{-2} \text{ s}^{-1}$), many *C. reinhardtii* cells lacked
15 partial or whole lobes (the regions extending from the base of the cup-shaped chloroplast toward
16 the flagella at the anterior of the cell; Figure 4d). Under HL, the patchy membrane surface
17 patterns became unclear due to the loss of the lobes. However, we observed the recovery of the
18 lobes within one day after returning the cells to LL conditions (Figure S5a). We also observed a
19 similar lobe shrinking phenotype in the *npq4 lhcsr1* mutant, which lacks the qE type of
20 non-photochemical quenching (NPQ) mechanisms, grown photoautotrophically under HL (Figure
21 S5b) (Ballottari *et al.* 2016). This result suggests that the lobe shrinking process is independent
22 of qE mechanisms. It has been suggested that the lobe region contains photosynthetically active
23 thylakoid membranes with fully assembled PSII-LHCII supercomplexes, while the basal region
24 contains biogenic membranes where protein synthesis and membrane biogenesis take place
25 (Schottkowski *et al.* 2012). We hypothesize that the shrinking of thylakoid membranes at the lobe
26 region decreases light absorption under HL and could prevent immediate photodamage from
27 occurring at the basal region.
28
29
30
31
32
33
34
35
36
37
38
39
40

41 **Visualizing other organelles and photosynthetic organisms using 3D-SIM.**

42 Using chemical labeling techniques, SIM is readily capable of visualizing nonfluorescent
43 organelles. For example, we used MitoTracker to stain mitochondria in *C. reinhardtii*, which are
44 known to change morphology during the life cycle. We stained and observed cells grown
45 heterotrophically under DL. Reconstructed 3D-SIM images confirmed the tubular structure of the
46 mitochondrial network (Figure 5a) that has been frequently observed at the end of the light
47 period during the day/night cycle (Ehara *et al.* 1995). Optical sectioning of 3D-SIM reconstructed
48 images indicated that the tubular mitochondrial structure was continuous and located close to the
49 surface of the chloroplast (Figure 5c). Furthermore, we used BODIPY to stain neutral lipids in the
50 *C. reinhardtii* cells under nitrogen starvation. 3D-SIM reconstructed images showed the
51
52
53
54
55
56
57
58
59
60

1
2
3 formation of neutral lipid droplets located in close proximity to the chloroplast envelope (Figure
4 5b), which is similar to what has been observed by EM (Goodson *et al.* 2011, Moriyama *et al.*
5 2018). However, the location of the lipid droplets makes it difficult to distinguish whether they are
6 in the chloroplast or cytosol. Interestingly, the optical sectioning and reconstructed 3D-SIM
7 images revealed connections between some lipid droplets (Figure 5d). Additionally under
8 nitrogen starvation conditions, Chl fluorescence of thylakoid structure and organization was
9 greatly disrupted (Figure 5b). These results suggest that morphological changes in the
10 mitochondrial network and formation of lipid droplets, in conjunction with thylakoid structure and
11 organization, can be visualized at subdiffraction resolution by the time-lapse 3D-SIM analysis.

12
13 To seek wider applicability of 3D-SIM to other organisms, we investigated the green
14 alga *Chromochloris zofingiensis*. *C. zofingiensis* shows an increase in accumulation of
15 astaxanthin and lipids under a variety of conditions including heterotrophy (Mulders *et al.* 2014,
16 Zhang *et al.* 2016, Roth *et al.* 2017). Staining heterotrophic cells with BODIPY and imaging with
17 3D-SIM revealed cytosolic lipid bodies accumulating near the periphery of the cell (Figure 5e).
18 The reconstructed 3D-SIM images also showed irregular shapes of thylakoid membranes in the
19 heterotrophically grown cell (Figure 5e).

20
21 Furthermore, we also tested the capability of 3D-SIM with protonema cells from the
22 moss *P. patens*. We grew *P. patens* protonema on agar medium without or with glucose. *P.*
23 *patens* grown without glucose is known to induce chloronema cells, which contain more
24 chloroplasts, while *P. patens* grown with glucose induces caulonema cells, which contain fewer
25 chloroplasts (Schumaker and Dietrich 1997, Olsson *et al.* 2003). The reconstructed 3D-SIM
26 images showed distinct grana structures in the chloroplasts in the chloronema cell (Figure 5f),
27 while the chloroplasts in the caulonema cell did not have well-defined grana structures (Figure
28 5g). We observed mitochondria in both types of protonema cells by using MitoTracker. The
29 reconstructed 3D-SIM images indicated that mitochondria in the caulonema cell appeared to be
30 longer and more tubular than in the chloronema cell (Figure 5f,g). This change in mitochondrial
31 structure may be correlated with the energy supply, which is known to control the balance
32 between chloronema and caulonema cells (Thelander *et al.* 2005).

33 DISCUSSION

34 Chloroplasts are readily observable by fluorescence microscopy as small, distinct, and
35 autofluorescent organelles in photosynthetic organisms. However, visualizing and resolving
36 structures inside chloroplasts *in vivo* is challenging because of the bright Chl fluorescence from
37 numerous photosynthetic membrane proteins in the intricate thylakoid membrane structures
38
39
40
41
42
43
44
45
46
47
48

1
2
3 within a 5–10 μm size organelle (Figures 1a, 2a,c). In this study, we utilized 3D-SIM to visualize
4 the structural organization of thylakoid membranes in chloroplasts. Our observations
5 demonstrate that 3D-SIM provides the capacity to investigate the detailed network of thylakoid
6 membranes in the chloroplasts of *A. thaliana* and *C. reinhardtii in vivo*. Our results indicate that
7 the spatial resolution of the reconstructed 3D-SIM images is not sufficient to distinguish each
8 individual layer within a stack of thylakoid membranes, which is 15.7 nm for *A. thaliana* and 22.4
9 nm for *C. reinhardtii* as observed by cryo-ET (Kirchhoff, *et al.* 2011, Engel, *et al.* 2015).
10 Nevertheless, our results suggest that the differences in thylakoid membrane characteristics in
11 different mutants and under different growth conditions can be distinguished and analyzed in
12 reconstructed 3D-SIM images (Figures 1, 2, 4). Recently, isolated chloroplasts from spinach
13 have also been observed by 3D-SIM, showing the smaller and larger grana sizes in response to
14 light and dark conditions, which are caused by phosphorylation and dephosphorylation of LHCII
15 (Wood, *et al.* 2018).

16 A major advantage of using optical microscopy is that no sample sectioning is required
17 to acquire the images, which allows us to observe a wide volumetric range of intact samples via
18 optical serial sectioning. With the subdiffraction spatial resolution achieved by 3D-SIM, it is
19 possible to visualize thylakoid characteristics in a whole chloroplast by a nondestructive method
20 (Figures S1–S4). Our observations indicate that there are structural variations in thylakoid
21 characteristics in each chloroplast even within the same strain under the same condition (Figures
22 1g-k, 2f, 4a,b). With 3D-SIM, it is manageable to analyze a large number of samples to reveal
23 structural characteristics of thylakoids *in vivo* with statistical support, which is often too
24 time-consuming for EM. Moreover, EM requires fixing and staining samples as opposed to *in vivo*
25 or near native state of chloroplasts used for 3D-SIM. Altogether, this study shows that 3D-SIM is
26 a valuable method to obtain high-resolution images and analyze a large number of *in vivo* or near
27 native state chloroplasts to elucidate thylakoid membrane dynamics and more.

28 It is worth mentioning drawbacks of using 3D-SIM. To reconstruct a 3D-SIM image at
29 subdiffraction resolution, it requires capturing at least 15 images (images excited with 5 different
30 phase-shifted patterns of light at 3 different angles of rotation) (Demmerle, *et al.* 2017). With our
31 3D-SIM system, it takes ~ 10 ms to acquire a raw image of Chl fluorescence (512×512 pixels)
32 and roughly ~ 4 s to acquire a volumetric image containing 10 sequential focal planes with 100
33 nm z-intervals. As is always a concern with types of laser microscopy observation, a certain level
34 of photodamage can occur and must be assessed with a series of control experiments when
35 conducting time-lapse 3D-SIM analyses. Also, it is essential to adjust the instrument settings and
36 optimize imaging conditions to avoid artifacts during image reconstruction, which are often when
37
38
39
40
41
42
43
44
45
46
47
48
49
50
51
52
53
54
55
56
57
58
59
60

1
2
3 fluorescence signals are low and non-modulated noise signals interfere with real structures. The
4 blurred hexagonal repeating signals, in particular outside the main Chl fluorescence signal, of the
5 thylakoid surface membrane structures in *C. reinhardtii* (Figure 4c, slice number 1) is an example
6 of an artifact. This artifact is due not only to the weak signals, but also the optical aberration
7 caused by the curved cell surface with different refractive properties. To evaluate the quality of
8 the reconstructed 3D-SIM images, programs such as *SIMcheck* (Ball *et al.* 2015) for ImageJ are
9 helpful. It is sometimes impractical to prevent optical aberration from occurring because of the
10 strong Chl fluorescence from an oval shaped object of 5-10 μm size such as chloroplasts and *C.*
11 *reinhardtii* cells; therefore, it is also important to evaluate the presence of an artifact by
12 examining each sequential focal plane in a reconstructed 3D-SIM image.
13
14
15
16
17
18

19 In general, there are several caveats for live-cell imaging of chloroplasts and thylakoid
20 membranes. As mentioned earlier, it is often practical to assume that the structures visualized by
21 Chl fluorescence indicate thylakoid membranes, which are filled with Chl-binding membrane
22 proteins. However, it is important to keep in mind that Chl fluorescence is not emitted directly by
23 the thylakoid membranes themselves. Chl fluorescence intensity can also be affected by many
24 factors such as NPQ induction and the redox state of plastoquinone pools in thylakoid
25 membranes. We observed the shrinkage of fluorescent thylakoid structures at the lobe region in
26 *C. reinhardtii* chloroplasts under HL conditions (Figure 4d), but this technique cannot distinguish
27 whether thylakoid membranes were lost from the lobes or whether they remain but lost Chl
28 fluorescence emission due to HL stress. 3D-SIM of Chl fluorescence also cannot determine the
29 location of or changes in the chloroplast envelope. Furthermore, it is known that the level of Chl
30 fluorescence emission from PSI is much lower than that of PSII at room temperature.
31 Fluorescence microscopy imaging conditions generally adjust the detection sensitivity to the
32 highest signal (*i.e.*, PSII fluorescence) observed in the field of view. Therefore, when imaging Chl
33 fluorescence at room temperature without spectral and/or fluorescence lifetime imaging, PSI
34 fluorescence is often nearly invisible in acquired images. However, the benefits of 3D-SIM and its
35 capacity to visualize whole chloroplasts *in vivo* at high-resolution offers possibilities to provide
36 insights into thylakoid membrane dynamics.
37
38
39
40
41
42
43
44
45
46
47
48

49 CONCLUSION

50 Observations of chloroplast membrane structure at high spatial resolution *in vivo* will improve
51 understanding of thylakoid membrane dynamics. This study demonstrates the capacity of
52 3D-SIM to differentiate general thylakoid membrane characteristics using nondestructive
53 techniques. In future studies, these findings can be applied to investigate thylakoid membrane
54
55
56
57
58
59
60

1
2
3 dynamics. Technological improvements in 3D-SIM could enable visualization of individual layers
4 of thylakoid membranes. In addition to the subdiffraction spatial resolution provided by 3D-SIM,
5 increasing temporal resolution (Chen *et al.* 2014, Hayashi and Okada 2015) will also be essential
6 to further explore thylakoid dynamics. Moreover, developments in deconvolution algorithms to
7 reconstruct accurate images with very low signals (Arigovindan *et al.* 2013) will be critical to
8 reduce phototoxicity for time-lapse imaging. Developing imaging techniques to visualize
9 thylakoid dynamics will provide not only understanding of the regulation of photosynthesis at
10 unprecedented spatiotemporal scales, but also expand the possibilities to investigate other
11 molecular activities occurring in chloroplasts of photosynthetic organisms.
12
13
14
15
16
17
18

19 **EXPERIMENTAL PROCEDURES**

20 **Strains and growth conditions**

21 *A. thaliana* WT (ecotype Columbia-0), *stn7 stn8* (Fristedt, *et al.* 2009) and *tap38* (Pribil, *et al.*
22 2010) were grown on soil under $\sim 100 \mu\text{mol photons m}^{-2} \text{ s}^{-1}$ with light (10 h) and dark (14 h) cycles
23 at 21 °C for 4-5 weeks. *C. reinhardtii* WT (4A+) (Dent *et al.* 2005) was grown either
24 photoautotrophically in minimal HS liquid medium or heterotrophically in acetate-containing TAP
25 liquid medium under continuous LL conditions ($\sim 50 \mu\text{mol photons m}^{-2} \text{ s}^{-1}$) as described
26 previously (Baroli *et al.* 2004). Different light treatments included continuous DL ($\sim 5 \mu\text{mol}$
27 photons $\text{m}^{-2} \text{ s}^{-1}$) and continuous HL ($\sim 350 \mu\text{mol photons m}^{-2} \text{ s}^{-1}$) conditions. For nitrogen
28 starvation conditions, the culture at mid-exponential growth phase in TAP liquid medium was
29 transferred to medium without nitrogen source and grown under LL conditions for 3 days. *C.*
30 *zofingiensis* WT (SAG 211-14) was grown heterotrophically in Proteose medium (UTEX Culture
31 Collection of Algae) with Chu's micronutrient solution and 10 mM glucose under $\sim 100 \mu\text{mol}$
32 photons $\text{m}^{-2} \text{ s}^{-1}$ with light (16 h) and dark (8 h) cycles at 25 °C as described previously (Roth, *et al.*
33 2017). *P. patens* WT (Gransden 2004) protonema were grown on a layer of cellophane overlaid
34 on BCDAT agar medium without or with glucose (5 g/L) (Nishiyama *et al.* 2000) at 25 °C under
35 continuous light at $\sim 50 \mu\text{mol photons m}^{-2} \text{ s}^{-1}$.
36
37
38
39
40
41
42
43
44
45
46

47 **3D-SIM sample preparation**

48 The chloroplasts in *A. thaliana* mesophyll tissues (Figure 1) were observed by removing the
49 lower epidermal tissues using tape. The leaf tissues were covered with water placed between
50 two coverslips attached in an Attolfluor cell chamber (Thermo Fisher Scientific). To observe the
51 side-view chloroplasts (Figure 2), chloroplasts were isolated from *A. thaliana* leaves as
52 previously described (Mizusawa *et al.* 1999), except that only 40% Percoll (no 80%) was used to
53
54
55
56
57
58
59
60

1
2
3 sediment the intact chloroplasts at 3,000 x g for 5 min for quick purification. The intact
4 chloroplasts in the pellet, washed once with 0.03 M HEPES (pH 7.8) and 0.33 M sorbitol at 3,000
5 x g for 5 min, were resuspended with the 0.5% low-melting point agarose in Murashige and
6 Skoog medium and mounted between two coverslips placed in an Attofluor cell chamber for
7 3D-SIM observation. To prepare *C. reinhardtii* cells for microscopy (Figures 3, 4), the cultures
8 grown under designated conditions were centrifuged at 3,000 x g and room temperature for 1
9 min. The pelleted cells were resuspended with 0.5% low-melting point agarose in appropriate
10 media (TAP or HS) and mounted between two coverslips placed in an Attofluor cell chamber for
11 3D-SIM observation. For staining the mitochondria in *C. reinhardtii* (Figure 5a,c), the pelleted
12 cells were resuspended with TAP liquid medium containing 1 μ M MitoTracker Orange CMTMRos
13 (Thermo Fisher Scientific). The cells were incubated in the dark for 30 min, and washed with TAP
14 liquid medium without dye three times at the same centrifuge conditions as above. For staining
15 neutral lipids in *C. reinhardtii* cells under nitrogen starvation (Figure 5b,d), the pelleted cells were
16 resuspended with TAP liquid medium without nitrogen source containing 5 μ g/mL BODIPYTM
17 493/503 dye (Invitrogen). The cells were incubated in the dark for 10 min, and washed with TAP
18 liquid medium without dye three times with the same centrifuge conditions as above. For staining
19 neutral lipids in the *C. zofingiensis* cells under heterotrophic growth conditions (Figure 5e), the
20 same BODIPY staining protocol as *C. reinhardtii* was used, except that Proteose liquid medium
21 was used. For staining the mitochondria in *P. patens* cells (Figure 5f,g), protonema grown on
22 BCDAT agar medium with or without glucose were incubated with 0.5 μ M MitoTracker Orange
23 CMTMRos in the dark for 30 min. The protonema cells were then washed with 5 mL of water and
24 mounted directly on a coverslip.
25
26
27
28
29
30
31
32
33
34
35
36
37
38

39 **3D-SIM**

40
41 The microscopy samples were observed using an Elyra PS.1 SIM microscope (Zeiss) with
42 objective lens alpha Plan-Apochromat 100x/1.46 oil. Chl, MitoTracker, and BODIPY were excited
43 with 642, 561, and 488 nm laser, respectively, and fluorescence was acquired through a 655 nm
44 longpass filter, a 570-620 nm bandpass filter, and a 495-550 nm bandpass filter, respectively.
45 The image acquisition was done as fully controlled by ZEN software (Zeiss). One focal plane for
46 each 3D-SIM image was obtained by sequential fluorescence image acquisitions via the
47 excitation with the patterned light of 3 rotated angled, each of which contains 5 phases shifted.
48 The z-interval distance was 101 nm. Raw images were processed to reconstruct 3D images
49 using ZEN software. Extraction of the intensity data from each focal plane was performed using
50 the *SIMcheck* plugin (Ball, *et al.* 2015) for ImageJ software (US National Institutes of Health).
51
52
53
54
55
56
57
58
59
60

1
2
3 Peak fitting and FWHM measurements were done using the multipeak fit analysis packages in
4 Igor Pro software (WaveMetrics).
5
6
7

8 **ACKNOWLEDGEMENTS**

9 We thank Drs. Denise Schichnes and Steven Ruzin for the technical setup and maintenance for
10 Carl Zeiss Elyra PS.1 SIM, which was supported in part by the National Institutes of Health S10
11 program 1S10OD018136-01. This work was supported by the U.S. Department of Energy, Office
12 of Science, through the Photosynthetic Systems program in the Office of Basic Energy Sciences.
13 The experiments with *C. zofingiensis* were supported by the U.S. Department of Energy, Office of
14 Science, Office of Biological and Environmental Research, under Award Number
15 DE-SC0018301. K.K.N. is an investigator of the Howard Hughes Medical Institute.
16
17
18
19
20
21

22 **CONFLICT OF INTEREST**

23 The authors declare no conflict of interest.
24
25
26

27 **SUPPORTING INFORMATION**

28 Additional Supporting Information may be found in the online version of this article.

29
30 **Figure S1.** Optical sections of reconstructed 3D-SIM images of the side-view of the chloroplast
31 isolated from *A. thaliana* WT leaves.
32
33

34 **Figure S2.** Optical sections of reconstructed 3D-SIM images of the side-view of the chloroplast
35 isolated from *A. thaliana stn7 stn8* mutant leaves.
36

37 **Figure S3.** Optical sections of reconstructed 3D-SIM images of the side-view of the chloroplast
38 isolated from *A. thaliana tap38* mutant leaves.
39

40 **Figure S4.** Optical sections of reconstructed 3D-SIM images of WT *C. reinhardtii* cell.

41 **Figure S5.** Additional reconstructed 3D-SIM images showing shrinkage of thylakoid membranes
42 at the lobe region of *C. reinhardtii* chloroplasts under HL conditions for one day.
43
44
45
46
47
48
49
50
51
52
53
54
55
56
57
58
59
60

Figure Legends

Figure 1. The subdiffraction-resolution live-cell imaging analysis of the grana size of *A. thaliana* chloroplasts.

Chl fluorescence from *A. thaliana* chloroplasts in the mesophyll tissue observed and analyzed by 3D-SIM. As compared with the reconstructed widefield image (a), reconstructed 3D-SIM image (b) of chloroplasts in the WT showed distinct round shape structures, indicating the individual grana. The reconstructed 3D-SIM images of chloroplasts in (b) the WT control, (c) the *stn7 stn8* mutant, (d) the *tap38* mutant, and the WT acclimated to (e) far-red (FR) light, and (f) blue light (BL) conditions were analyzed to measure the differences in the grana size. Scale bars, 5 μm . FWHM of grana from (g) the WT control (n = 300 from 8 chloroplasts), (h) the *stn7 stn8* mutant (n = 124 from 8 chloroplasts), (i) the *tap38* mutant (n = 251 from 8 chloroplasts), and the WT chloroplasts acclimated to (j) FR light (n = 149 from 8 chloroplasts) or (k) BL (n = 172 from 8 chloroplasts). Inset numbers indicate mean FWHM \pm SD of all chloroplasts, and data represent means \pm SD for each chloroplast.

Figure 2. The reconstructed 3D-SIM images of the side-view of *A. thaliana* chloroplasts showing the thylakoid membrane architecture.

Chl fluorescence from isolated *A. thaliana* chloroplasts observed by 3D-SIM. Optical sections of chloroplasts isolated from (a) WT, (b) *stn7 stn8*, and (c) *tap38* are shown whole (left column) and enlarged to show detail (right column). Each number corresponds to the selected focal plane of the serial optical sections as shown in Figures S1–3. Scale bars, 1 μm . (d) Representative close-up image of a chloroplast side-view with a line scan for a thickness analysis of thylakoid membranes. (e) The intensity profile of the line indicated in (d) (top panel). The dotted line is the multipeak fit, which is used to extract the Gaussian distribution of each peak (bottom panel). The number indicates FWHM (μm) measured in each Gaussian distribution. (f) Thylakoid membrane length in chloroplasts of WT (n = 173 from 8 chloroplasts), *stn7 stn8* (n = 144 from 8 chloroplasts), and *tap38* (n = 156 from 8 chloroplasts). Inset numbers indicate mean FWHM \pm SD of all chloroplasts, and data represent means \pm SD for each chloroplast.

Figure 3. The subdiffraction-resolution live-cell imaging analysis of *C. reinhardtii* chloroplasts.

Chl fluorescence from *C. reinhardtii* chloroplasts observed by 3D-SIM. As compared to reconstructed widefield images (a,c), reconstructed 3D-SIM images (b,d) of *C. reinhardtii*

1
2
3 chloroplasts revealed the distinct thylakoid membrane structures. Arrows and arrowheads in (d)
4 indicate the basal and lobe regions, respectively. (e) Selected optical sections of close-up
5 3D-SIM images showing the basal region of the chloroplast as shown in (d). Each number
6 corresponds to the selected focal plane of the serial optical sections as shown in Figure S4.
7 Arrows in (e) indicate thylakoid membranes, which appeared to extend into the pyrenoid. (f)
8 Detail image of the thylakoid tip convergence region. (g) The intensity profile of the line indicated
9 in (f). The dotted line is the multipeak fit, which was used to extract the Gaussian distribution of
10 each peak as shown at the bottom. The number indicates FWHM (nm) measured in each
11 Gaussian distribution. Scale bars, 10 μm (a,b), 2 μm (c–f).
12
13
14
15
16
17
18
19

20 **Figure 4.** Structural comparison of thylakoid structures in the *C. reinhardtii* cells grown under
21 different conditions.

22
23 Chl fluorescence from chloroplasts of *C. reinhardtii* observed by 3D-SIM. Reconstructed 3D-SIM
24 images of Chl fluorescence showing paired central (top image) and peripheral (bottom image)
25 focal planes of (a) heterotrophically and (b) photoautotrophically grown cells under dim light
26 conditions ($\sim 5 \mu\text{mol photons m}^{-2} \text{ s}^{-1}$). Optical sections from the peripheral to central focal planes
27 of photoautotrophically grown cell under (c) low light ($\sim 50 \mu\text{mol photons m}^{-2} \text{ s}^{-1}$) and (d) high light
28 ($\sim 350 \mu\text{mol photons m}^{-2} \text{ s}^{-1}$) conditions. The numbers indicate selected focal planes of the optical
29 sections. Scale bars, 2 μm .
30
31
32
33
34
35
36

37 **Figure 5.** Reconstructed 3D-SIM images of other organelles and photosynthetic organisms.

38 (a) The mitochondria in heterotrophically grown *C. reinhardtii* cells were stained by MitoTracker
39 (MT) and observed by 3D-SIM. Top, Chl; middle, MT; bottom, merged. (b) Lipid droplets in *C.*
40 *reinhardtii* cells under nitrogen starvation were stained by BODIPY and observed by 3D-SIM. Top,
41 Chl; middle, BODIPY; bottom, merged. (c) MT fluorescence in selected optical sections from the
42 peripheral to central focal planes of the cell as shown in (a). (d) BODIPY fluorescence in the
43 selected optical sections from the peripheral to central focal planes of the cell as shown in (b).
44 Arrows indicate a lipid droplet connecting to another one in the different focal planes. (e) Lipid
45 bodies in heterotrophically grown *C. zofingiensis* cell were stained by BODIPY and observed by
46 3D-SIM. Top, Chl; middle, BODIPY; bottom, merged. Mitochondria in (f) the chloronema cell and
47 (g) the caulonema cell of *P. patens* were stained by MT and observed by 3D-SIM. Left, Chl;
48
49
50
51
52
53
54
55
56
57
58
59
60

1
2
3 middle, MT; right, merged. Numbers indicate the selected focal planes of the serial optical
4 sections. Scale bars, 2 μm (a–e), 5 μm (f, g).
5
6
7

8 REFERENCES

9

- 10
11
12 **Arigovindan, M., Fung, J.C., Elnatan, D., Mennella, V., Chan, Y.H., Pollard, M., Branlund, E., Sedat,**
13 **J.W. and Agard, D.A.** (2013) High-resolution restoration of 3D structures from widefield images
14 with extreme low signal-to-noise-ratio. *Proc. Natl Acad. Sci. USA*, **110**, 17344-17349.
15
16
17 **Armbruster, U., Labs, M., Pribil, M., Viola, S., Xu, W., Scharfenberg, M., Hertle, A.P., Rojahn, U.,**
18 **Jensen, P.E., Rappaport, F., Joliot, P., Dormann, P., Wanner, G. and Leister, D.** (2013)
19 *Arabidopsis* CURVATURE THYLAKOID1 proteins modify thylakoid architecture by inducing
20 membrane curvature. *Plant Cell*, **25**, 2661-2678.
21
22
23 **Austin, J.R., 2nd and Staehelin, L.A.** (2011) Three-dimensional architecture of grana and stroma
24 thylakoids of higher plants as determined by electron tomography. *Plant Physiol.*, **155**, 1601-1611.
25
26
27 **Ball, G., Demmerle, J., Kaufmann, R., Davis, I., Dobbie, I.M. and Schermelleh, L.** (2015) SIMcheck: a
28 toolbox for successful super-resolution structured illumination microscopy. *Sci. Rep.*, **5**, 15915.
29
30
31 **Ballottari, M., Truong, T.B., De Re, E., Erickson, E., Stella, G.R., Fleming, G.R., Bassi, R. and Niyogi,**
32 **K.K.** (2016) Identification of pH-sensing sites in the light harvesting complex stress-related 3
33 protein essential for triggering non-photochemical quenching in *Chlamydomonas reinhardtii*. *J.*
34 *Biol. Chem.*, **291**, 7334-7346.
35
36
37 **Baroli, I., Gutman, B.L., Ledford, H.K., Shin, J.W., Chin, B.L., Havaux, M. and Niyogi, K.K.** (2004)
38 Photo-oxidative stress in a xanthophyll-deficient mutant of *Chlamydomonas*. *J. Biol. Chem.*, **279**,
39 6337-6344.
40
41
42 **Beck, M. and Baumeister, W.** (2016) Cryo-electron tomography: Can it reveal the molecular sociology of
43 cells in atomic detail? *Trends Cell Biol.*, **26**, 825-837.
44
45
46 **Bellafore, S., Barneche, F., Peltier, G. and Rochaix, J.D.** (2005) State transitions and light adaptation
47 require chloroplast thylakoid protein kinase STN7. *Nature*, **433**, 892-895.
48
49
50 **Betterle, N., Ballottari, M., Zorzan, S., de Bianchi, S., Cazzaniga, S., Dall'osto, L., Morosinotto, T. and**
51 **Bassi, R.** (2009) Light-induced dissociation of an antenna hetero-oligomer is needed for
52 non-photochemical quenching induction. *J. Biol. Chem.*, **284**, 15255-15266.
53
54
55 **Bonardi, V., Pesaresi, P., Becker, T., Schleiff, E., Wagner, R., Pfannschmidt, T., Jahns, P. and Leister,**
56 **D.** (2005) Photosystem II core phosphorylation and photosynthetic acclimation require two
57
58
59
60

1
2
3 different protein kinases. *Nature*, **437**, 1179-1182.

4
5 **Caffarri, S., Broess, K., Croce, R. and van Amerongen, H.** (2011) Excitation energy transfer and
6 trapping in higher plant photosystem II complexes with different antenna sizes. *Biophys. J.*, **100**,
7 2094-2103.

8
9
10 **Chen, B.C., Legant, W.R., Wang, K., Shao, L., Milkie, D.E., Davidson, M.W., Janetopoulos, C., Wu,**
11 **X.S., Hammer, J.A., 3rd, Liu, Z., English, B.P., Mimori-Kiyosue, Y., Romero, D.P., Ritter, A.T.,**
12 **Lippincott-Schwartz, J., Fritz-Laylin, L., Mullins, R.D., Mitchell, D.M., Bembenek, J.N.,**
13 **Reymann, A.C., Bohme, R., Grill, S.W., Wang, J.T., Seydoux, G., Tulu, U.S., Kiehart, D.P. and**
14 **Betzig, E.** (2014) Lattice light-sheet microscopy: imaging molecules to embryos at high
15 spatiotemporal resolution. *Science*, **346**, 1257998.

16
17
18 **Demmerle, J., Innocent, C., North, A.J., Ball, G., Muller, M., Miron, E., Matsuda, A., Dobbie, I.M.,**
19 **Markaki, Y. and Schermelleh, L.** (2017) Strategic and practical guidelines for successful
20 structured illumination microscopy. *Nat. Protoc.*, **12**, 988-1010.

21
22
23 **Dent, R.M., Haglund, C.M., Chin, B.L., Kobayashi, M.C. and Niyogi, K.K.** (2005) Functional genomics
24 of eukaryotic photosynthesis using insertional mutagenesis of *Chlamydomonas reinhardtii*. *Plant*
25 *Physiol.*, **137**, 545-556.

26
27
28 **Ehara, T., Osafune, T. and Hase, E.** (1995) Behavior of mitochondria in synchronized cells of
29 *Chlamydomonas reinhardtii* (Chlorophyta). *J. Cell Sci.*, **108**, 499-507.

30
31
32 **Engel, B.D., Schaffer, M., Kuhn Cuellar, L., Villa, E., Plitzko, J.M. and Baumeister, W.** (2015) Native
33 architecture of the *Chlamydomonas* chloroplast revealed by in situ cryo-electron tomography. *eLife*,
34 **4**, e04889.

35
36
37 **Erickson, E., Wakao, S. and Niyogi, K.K.** (2015) Light stress and photoprotection in *Chlamydomonas*
38 *reinhardtii*. *Plant J.*, **82**, 449-465.

39
40
41 **Fristedt, R., Willig, A., Granath, P., Crevecoeur, M., Rochaix, J.D. and Vener, A.V.** (2009)
42 Phosphorylation of photosystem II controls functional macroscopic folding of photosynthetic
43 membranes in *Arabidopsis*. *Plant Cell*, **21**, 3950-3964.

44
45
46 **Goodson, C., Roth, R., Wang, Z.T. and Goodenough, U.** (2011) Structural correlates of cytoplasmic and
47 chloroplast lipid body synthesis in *Chlamydomonas reinhardtii* and stimulation of lipid body
48 production with acetate boost. *Eukaryot. Cell*, **10**, 1592-1606.

49
50
51 **Goral, T.K., Johnson, M.P., Duffy, C.D., Brain, A.P., Ruban, A.V. and Mullineaux, C.W.** (2012)
52 Light-harvesting antenna composition controls the macrostructure and dynamics of thylakoid
53 membranes in *Arabidopsis*. *Plant J.*, **69**, 289-301.

- 1
2
3
4 **Gustafsson, M.G., Shao, L., Carlton, P.M., Wang, C.J., Golubovskaya, I.N., Cande, W.Z., Agard, D.A.**
5 **and Sedat, J.W.** (2008) Three-dimensional resolution doubling in wide-field fluorescence
6 microscopy by structured illumination. *Biophys. J.*, **94**, 4957-4970.
- 7
8 **Haldrup, A., Jensen, P.E., Lunde, C. and Scheller, H.V.** (2001) Balance of power: a view of the
9 mechanism of photosynthetic state transitions. *Trends Plant Sci.*, **6**, 301-305.
- 10
11 **Hayashi, S. and Okada, Y.** (2015) Ultrafast superresolution fluorescence imaging with spinning disk
12 confocal microscope optics. *Mol. Biol. Cell*, **26**, 1743-1751.
- 13
14 **Heifetz, P.B., Förster, B., Osmond, C.B., Giles, L.J. and Boynton, J.E.** (2000) Effects of acetate on
15 facultative autotrophy in *Chlamydomonas reinhardtii* assessed by photosynthetic measurements
16 and stable isotope analyses. *Plant Physiol.*, **122**, 1439-1446.
- 17
18 **Horton, P., Ruban, A.V. and Walters, R.G.** (1996) Regulation of light harvesting in green plants. *Annu.*
19 *Rev. Plant Physiol. Plant Mol. Biol.*, **47**, 655-684.
- 20
21 **Iwai, M., Yokono, M., Kurokawa, K., Ichihara, A. and Nakano, A.** (2016) Live-cell visualization of
22 excitation energy dynamics in chloroplast thylakoid structures. *Sci. Rep.*, **6**, 29940.
- 23
24 **Iwai, M., Yokono, M. and Nakano, A.** (2014) Visualizing structural dynamics of thylakoid membranes. *Sci.*
25 *Rep.*, **4**, 3768.
- 26
27 **Johnson, M.P., Goral, T.K., Duffy, C.D., Brain, A.P., Mullineaux, C.W. and Ruban, A.V.** (2011)
28 Photoprotective energy dissipation involves the reorganization of photosystem II light-harvesting
29 complexes in the grana membranes of spinach chloroplasts. *Plant Cell*, **23**, 1468-1479.
- 30
31 **Kirchhoff, H., Hall, C., Wood, M., Herbstova, M., Tsabari, O., Nevo, R., Charuvi, D., Shimoni, E. and**
32 **Reich, Z.** (2011) Dynamic control of protein diffusion within the granal thylakoid lumen. *Proc. Natl*
33 *Acad. Sci. USA*, **108**, 20248-20253.
- 34
35 **Kouril, R., Wientjes, E., Bultema, J.B., Croce, R. and Boekema, E.J.** (2013) High-light vs. low-light:
36 effect of light acclimation on photosystem II composition and organization in *Arabidopsis thaliana*.
37 *Biochim. Biophys. Acta*, **1827**, 411-419.
- 38
39 **Mackinder, L.C.M., Chen, C., Leib, R.D., Patena, W., Blum, S.R., Rodman, M., Ramundo, S., Adams,**
40 **C.M. and Jonikas, M.C.** (2017) A spatial interactome reveals the protein organization of the algal
41 CO₂-concentrating mechanism. *Cell*, **171**, 133-147 e114.
- 42
43 **Mizusawa, N., Yamamoto, N. and Miyao, M.** (1999) Characterization of damage to the D1 protein of
44 photosystem II under photoinhibitory illumination in non-phosphorylated and phosphorylated
45 thylakoid membranes. *J. Photochem. Photobiol. B*, **48**, 97-103.
- 46
47 **Moriyama, T., Toyoshima, M., Saito, M., Wada, H. and Sato, N.** (2018) Revisiting the algal "chloroplast
48
49
50
51
52
53
54
55
56
57
58
59
60

- lipid droplet": the absence of an entity that is unlikely to exist. *Plant Physiol.*, **176**, 1519-1530.
- Mulders, K.J.M., Janssen, J.H., Martens, D.E., Wijffels, R.H. and Lamers, P.P.** (2014) Effect of biomass concentration on secondary carotenoids and triacylglycerol (TAG) accumulation in nitrogen-depleted *Chlorella zofingiensis*. *Algal Res.*, **6**, 8-16.
- Nelson, N.** (2011) Photosystems and global effects of oxygenic photosynthesis. *Biochim. Biophys. Acta*, **1807**, 856-863.
- Nishiyama, T., Hiwatashi, Y., Sakakibara, I., Kato, M. and Hasebe, M.** (2000) Tagged mutagenesis and gene-trap in the moss, *Physcomitrella patens* by shuttle mutagenesis. *DNA Res.*, **7**, 9-17.
- Niyogi, K.K.** (1999) Photoprotection revisited: genetic and molecular approaches. *Annu. Rev. Plant Physiol. Plant Mol. Biol.*, **50**, 333-359.
- Olsson, T., Thelander, M. and Ronne, H.** (2003) A novel type of chloroplast stromal hexokinase is the major glucose-phosphorylating enzyme in the moss *Physcomitrella patens*. *J. Biol. Chem.*, **278**, 44439-44447.
- Pribil, M., Pesaresi, P., Hertle, A., Barbato, R. and Leister, D.** (2010) Role of plastid protein phosphatase TAP38 in LHCII dephosphorylation and thylakoid electron flow. *PLoS Biol.*, **8**, e1000288.
- Rochaix, J.D.** (2014) Regulation and dynamics of the light-harvesting system. *Annu. Rev. Plant Biol.*, **65**, 287-309.
- Roth, M.S., Cokus, S.J., Gallaher, S.D., Walter, A., Lopez, D., Erickson, E., Endelman, B., Westcott, D., Larabell, C.A., Merchant, S.S., Pellegrini, M. and Niyogi, K.K.** (2017) Chromosome-level genome assembly and transcriptome of the green alga *Chromochloris zofingiensis* illuminates astaxanthin production. *Proc. Natl Acad. Sci. USA*, **114**, E4296-E4305.
- Ruban, A.V.** (2016) Nonphotochemical chlorophyll fluorescence quenching: mechanism and effectiveness in protecting plants from photodamage. *Plant Physiol.*, **170**, 1903-1916.
- Schottkowski, M., Peters, M., Zhan, Y., Rifai, O., Zhang, Y. and Zerges, W.** (2012) Biogenic membranes of the chloroplast in *Chlamydomonas reinhardtii*. *Proc. Natl Acad. Sci. USA*, **109**, 19286-19291.
- Schumaker, K.S. and Dietrich, M.A.** (1997) Programmed changes in form during moss development. *Plant Cell*, **9**, 1099-1107.
- Shapiguzov, A., Ingelsson, B., Samol, I., Andres, C., Kessler, F., Rochaix, J.D., Vener, A.V. and Goldschmidt-Clermont, M.** (2010) The PPH1 phosphatase is specifically involved in LHCII dephosphorylation and state transitions in *Arabidopsis*. *Proc. Natl Acad. Sci. USA*, **107**, 4782-4787.

- 1
2
3
4 **Shimoni, E., Rav-Hon, O., Ohad, I., Brumfeld, V. and Reich, Z.** (2005) Three-dimensional organization
5 of higher-plant chloroplast thylakoid membranes revealed by electron tomography. *Plant Cell*, **17**,
6 2580-2586.
7
- 8 **Thelander, M., Olsson, T. and Ronne, H.** (2005) Effect of the energy supply on filamentous growth and
9 development in *Physcomitrella patens*. *J. Exp. Bot.*, **56**, 653-662.
10
- 11 **Valkunas, L., Chmeliov, J., Trinkunas, G., Duffy, C.D., van Grondelle, R. and Ruban, A.V.** (2011)
12 Excitation migration, quenching, and regulation of photosynthetic light harvesting in photosystem II.
13 *J. Phys. Chem. B*, **115**, 9252-9260.
14
- 15 **Wientjes, E., Drop, B., Kouril, R., Boekema, E.J. and Croce, R.** (2013) During state 1 to state 2
16 transition in *Arabidopsis thaliana*, the photosystem II supercomplex gets phosphorylated but does
17 not disassemble. *J. Biol. Chem.*, **288**, 32821-32826.
18
- 19 **Wobbe, L., Bassi, R. and Kruse, O.** (2016) Multi-level light capture control in plants and green algae.
20 *Trends Plant Sci.*, **21**, 55-68.
21
- 22 **Wood, W.H.J., MacGregor-Chatwin, C., Barnett, S.F.H., Mayneord, G.E., Huang, X., Hobbs, J.K.,**
23 **Hunter, C.N. and Johnson, M.P.** (2018) Dynamic thylakoid stacking regulates the balance
24 between linear and cyclic photosynthetic electron transfer. *Nat. Plants*, **4**, 116-127.
25
- 26 **Zhang, Z., Sun, D., Mao, X., Liu, J. and Chen, F.** (2016) The crosstalk between astaxanthin, fatty acids
27 and reactive oxygen species in heterotrophic *Chlorella zofingiensis*. *Algal Res.*, **19**, 178-183.
28
29
30
31
32
33
34
35
36
37
38
39
40
41
42
43
44
45
46
47
48
49
50
51
52
53
54
55
56
57
58
59
60

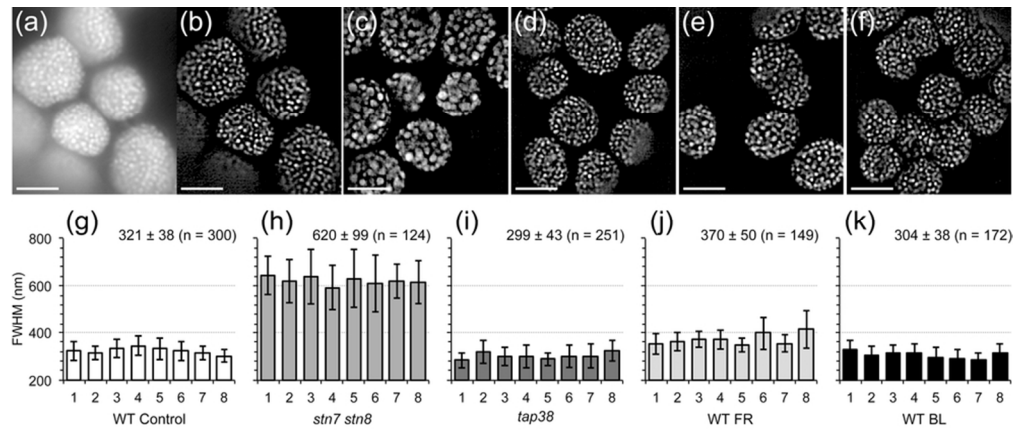


Figure 1. The subdiffraction-resolution live-cell imaging analysis of the grana size of *A. thaliana* chloroplasts. Chl fluorescence from *A. thaliana* chloroplasts in the mesophyll tissue observed and analyzed by 3D-SIM. As compared with the reconstructed widefield image (a), reconstructed 3D-SIM image (b) of chloroplasts in the WT showed distinct round shape structures, indicating the individual grana. The reconstructed 3D-SIM images of chloroplasts in (b) the WT control, (c) the *stn7 stn8* mutant, (d) the *tap38* mutant, and the WT acclimated to (e) far-red (FR) light, and (f) blue light (BL) conditions were analyzed to measure the differences in the grana size. Scale bars, 5 μ m. FWHM of grana from (g) the WT control (n = 300 from 8 chloroplasts), (h) the *stn7 stn8* mutant (n = 124 from 8 chloroplasts), (i) the *tap38* mutant (n = 251 from 8 chloroplasts), and the WT chloroplasts acclimated to (j) FR light (n = 149 from 8 chloroplasts) or (k) BL (n = 172 from 8 chloroplasts). Inset numbers indicate mean FWHM \pm SD of all chloroplasts, and data represent means \pm SD for each chloroplast.

83x35mm (300 x 300 DPI)

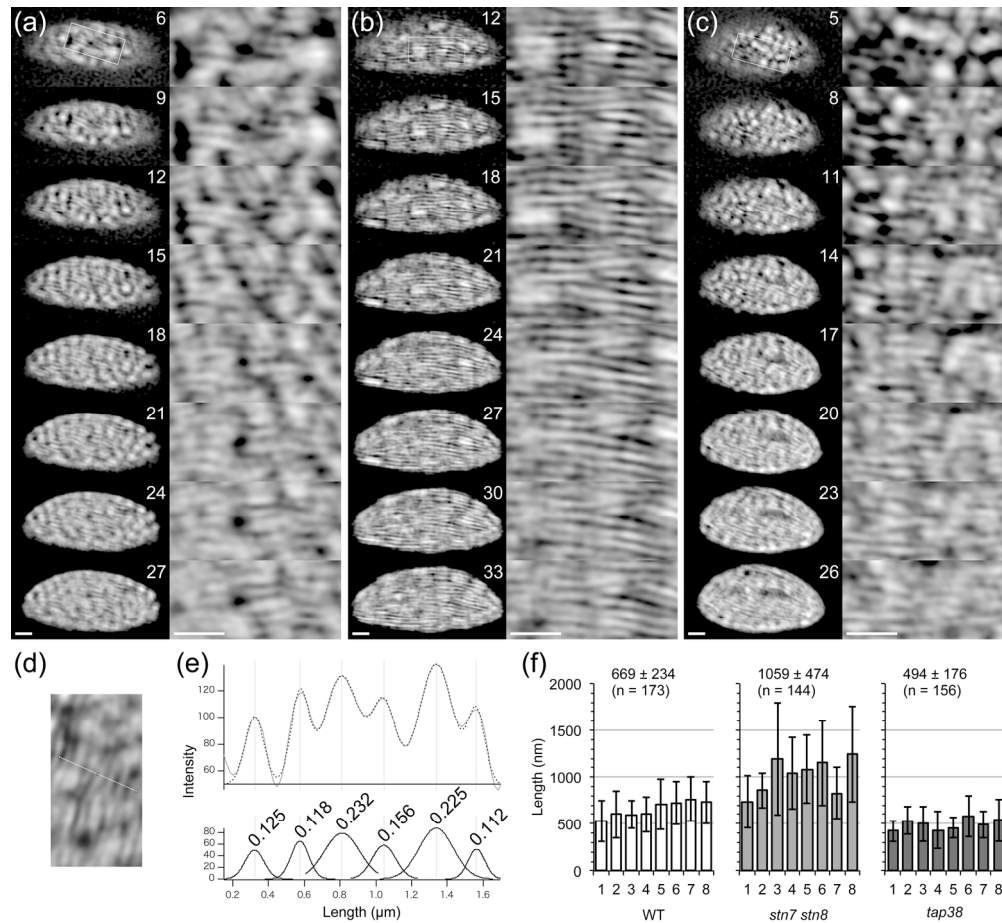


Figure 2. The reconstructed 3D-SIM images of the side-view of *A. thaliana* chloroplasts showing the thylakoid membrane architecture.

Chl fluorescence from isolated *A. thaliana* chloroplasts observed by 3D-SIM. Optical sections of chloroplasts isolated from (a) WT, (b) *stn7 stn8*, and (c) *tap38* are shown whole (left column) and enlarged to show detail (right column). Each number corresponds to the selected focal plane of the serial optical sections as shown in Figures S1–3. Scale bars, 1 μm . (d) Representative close-up image of a chloroplast side-view with a line scan for a thickness analysis of thylakoid membranes. (e) The intensity profile of the line indicated in (d) (top panel). The dotted line is the multipeak fit, which is used to extract the Gaussian distribution of each peak (bottom panel). The number indicates FWHM (μm) measured in each Gaussian distribution. (f) Thylakoid membrane length in chloroplasts of WT (n = 173 from 8 chloroplasts), *stn7 stn8* (n = 144 from 8 chloroplasts), and *tap38* (n = 156 from 8 chloroplasts). Inset numbers indicate mean FWHM \pm SD of all chloroplasts, and data represent means \pm SD for each chloroplast.

179x163mm (300 x 300 DPI)

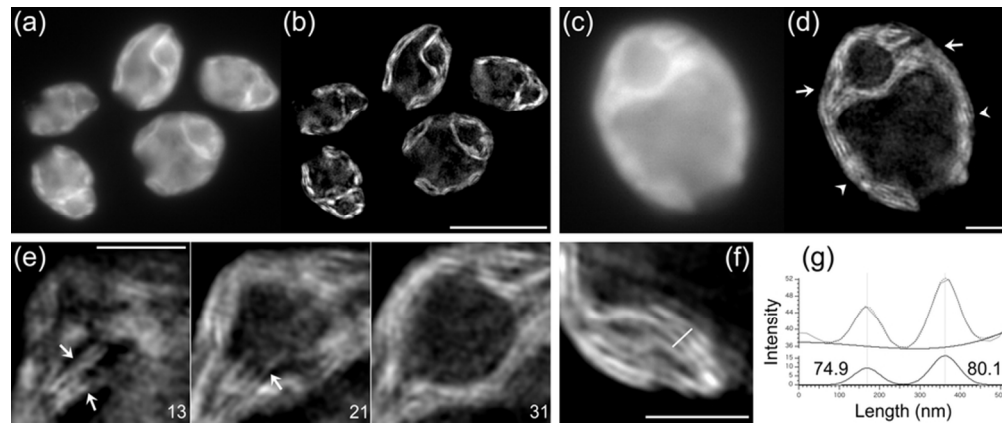


Figure 3. The subdiffraction-resolution live-cell imaging analysis of *C. reinhardtii* chloroplasts. Chl fluorescence from *C. reinhardtii* chloroplasts observed by 3D-SIM. As compared to reconstructed widefield images (a,c), reconstructed 3D-SIM images (b,d) of *C. reinhardtii* chloroplasts revealed the distinct thylakoid membrane structures. Arrows and arrowheads in (d) indicate the basal and lobe regions, respectively. (e) Selected optical sections of close-up 3D-SIM images showing the basal region of the chloroplast as shown in (d). Each number corresponds to the selected focal plane of the serial optical sections as shown in Figure S4. Arrows in (e) indicate thylakoid membranes, which appeared to extend into the pyrenoid. (f) Detail image of the thylakoid tip convergence region. (g) The intensity profile of the line indicated in (f). The dotted line is the multipeak fit, which was used to extract the Gaussian distribution of each peak as shown at the bottom. The number indicates FWHM (nm) measured in each Gaussian distribution. Scale bars, 10 μm (a,b), 2 μm (c-f).

81x33mm (300 x 300 DPI)

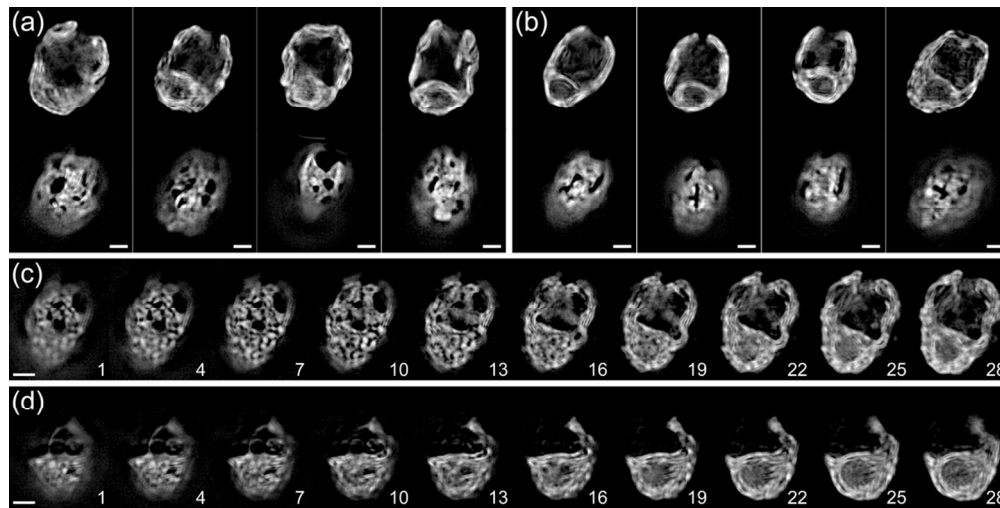


Figure 4. Structural comparison of thylakoid structures in the *C. reinhardtii* cells grown under different conditions.

Chl fluorescence from chloroplasts of *C. reinhardtii* observed by 3D-SIM. Reconstructed 3D-SIM images of Chl fluorescence showing paired central (top image) and peripheral (bottom image) focal planes of (a) heterotrophically and (b) photoautotrophically grown cells under dim light conditions ($\sim 5 \mu\text{mol photons m}^{-2} \text{s}^{-1}$). Optical sections from the peripheral to central focal planes of photoautotrophically grown cell under (c) low light ($\sim 50 \mu\text{mol photons m}^{-2} \text{s}^{-1}$) and (d) high light ($\sim 350 \mu\text{mol photons m}^{-2} \text{s}^{-1}$) conditions. The numbers indicate selected focal planes of the optical sections. Scale bars, $2 \mu\text{m}$.

98x49mm (300 x 300 DPI)

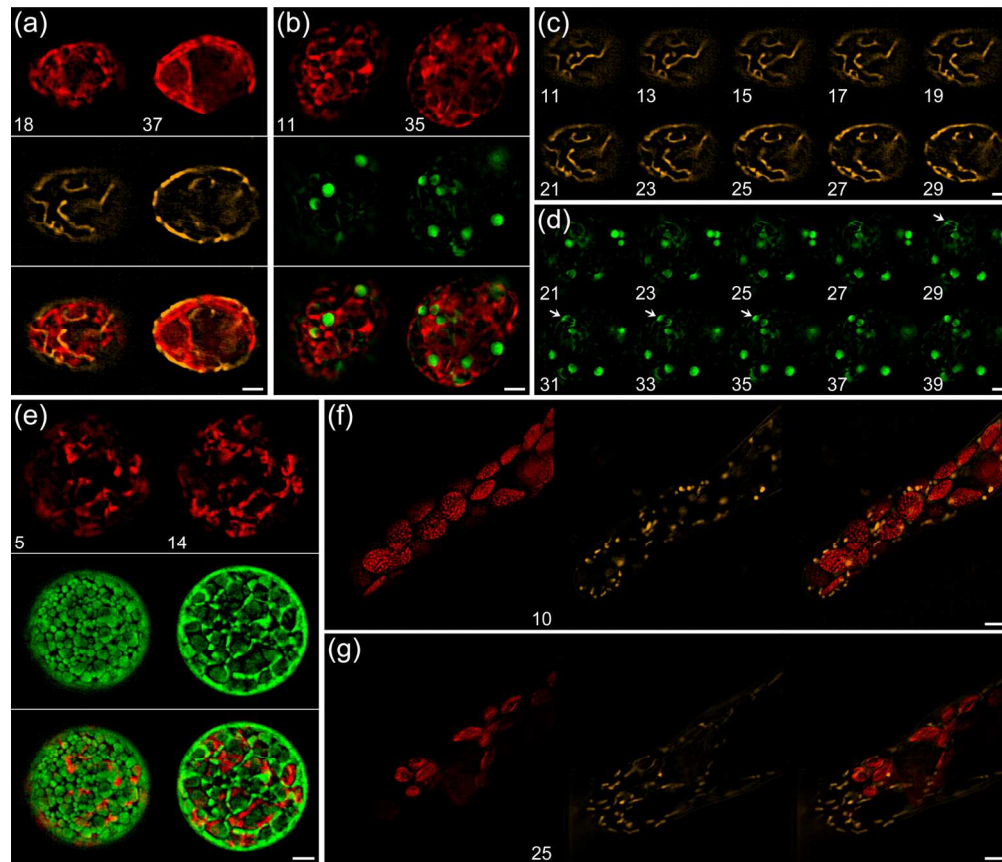


Figure 5. Reconstructed 3D-SIM images of other organelles and photosynthetic organisms.

(a) The mitochondria in heterotrophically grown *C. reinhardtii* cells were stained by MitoTracker (MT) and observed by 3D-SIM. Top, Chl; middle, MT; bottom, merged. (b) Lipid droplets in *C. reinhardtii* cells under nitrogen starvation were stained by BODIPY and observed by 3D-SIM. Top, Chl; middle, BODIPY; bottom, merged. (c) MT fluorescence in selected optical sections from the peripheral to central focal planes of the cell as shown in (a). (d) BODIPY fluorescence in the selected optical sections from the peripheral to central focal planes of the cell as shown in (b). Arrows indicate a lipid droplet connecting to another one in the different focal planes. (e) Lipid bodies in heterotrophically grown *C. zofingiensis* cell were stained by BODIPY and observed by 3D-SIM. Top, Chl; middle, BODIPY; bottom, merged. Mitochondria in (f) the chloronema cell and (g) the caulonema cell of *P. patens* were stained by MT and observed by 3D-SIM. Left, Chl; middle, MT; right, merged. Numbers indicate the selected focal planes of the serial optical sections. Scale bars, 2 μm (a–e), 5 μm (f, g).

163x140mm (300 x 300 DPI)

SUPPORTING INFORMATION

Subdiffraction-resolution live-cell imaging for visualizing thylakoid membranes

Masakazu Iwai*, Melissa S. Roth and Krishna K. Niyogi*

For correspondence (email miwai@berkeley.edu or niyogi@berkeley.edu).

TABLE OF CONTENTS

Figure S1. Optical sections of reconstructed 3D-SIM images of the side-view of the chloroplast isolated from *A. thaliana* WT leaves.

Figure S2. Optical sections of reconstructed 3D-SIM images of the side-view of the chloroplast isolated from *A. thaliana stn7 stn8* mutant leaves.

Figure S3. Optical sections of reconstructed 3D-SIM images of the side-view of the chloroplast isolated from *A. thaliana tap38* mutant leaves.

Figure S4. Optical sections of reconstructed 3D-SIM images of WT *C. reinhardtii* cell.

Figure S5. Additional reconstructed 3D-SIM images showing shrinkage of thylakoid membranes at the lobe region of *C. reinhardtii* chloroplasts under HL conditions for one day.

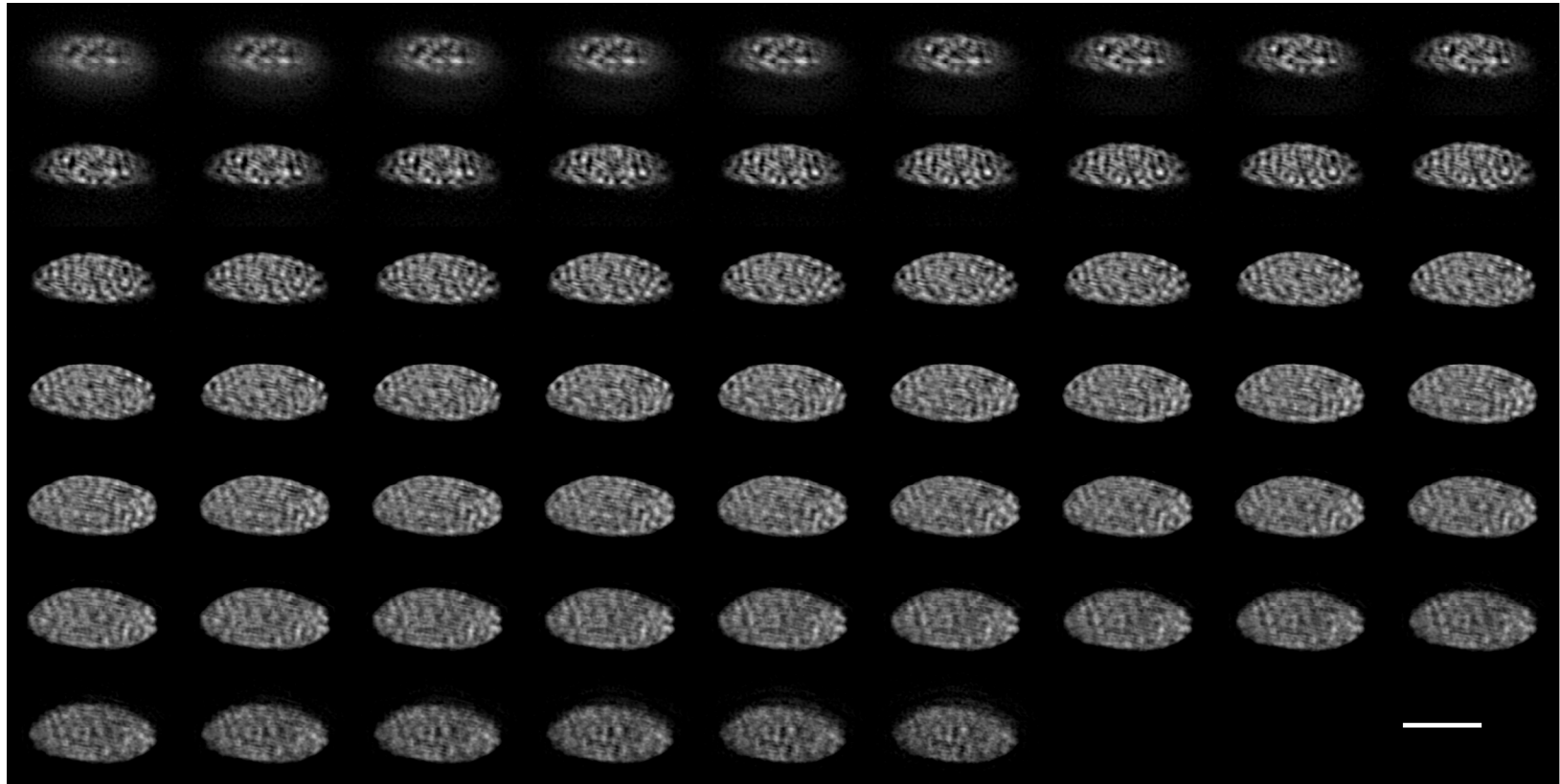


Figure S1. Optical sections of reconstructed 3D-SIM images of the side-view of the chloroplast isolated from *A. thaliana* WT leaves. The individual focal planes are shown in the order from top left to bottom right. Scale bar, 5 μm .

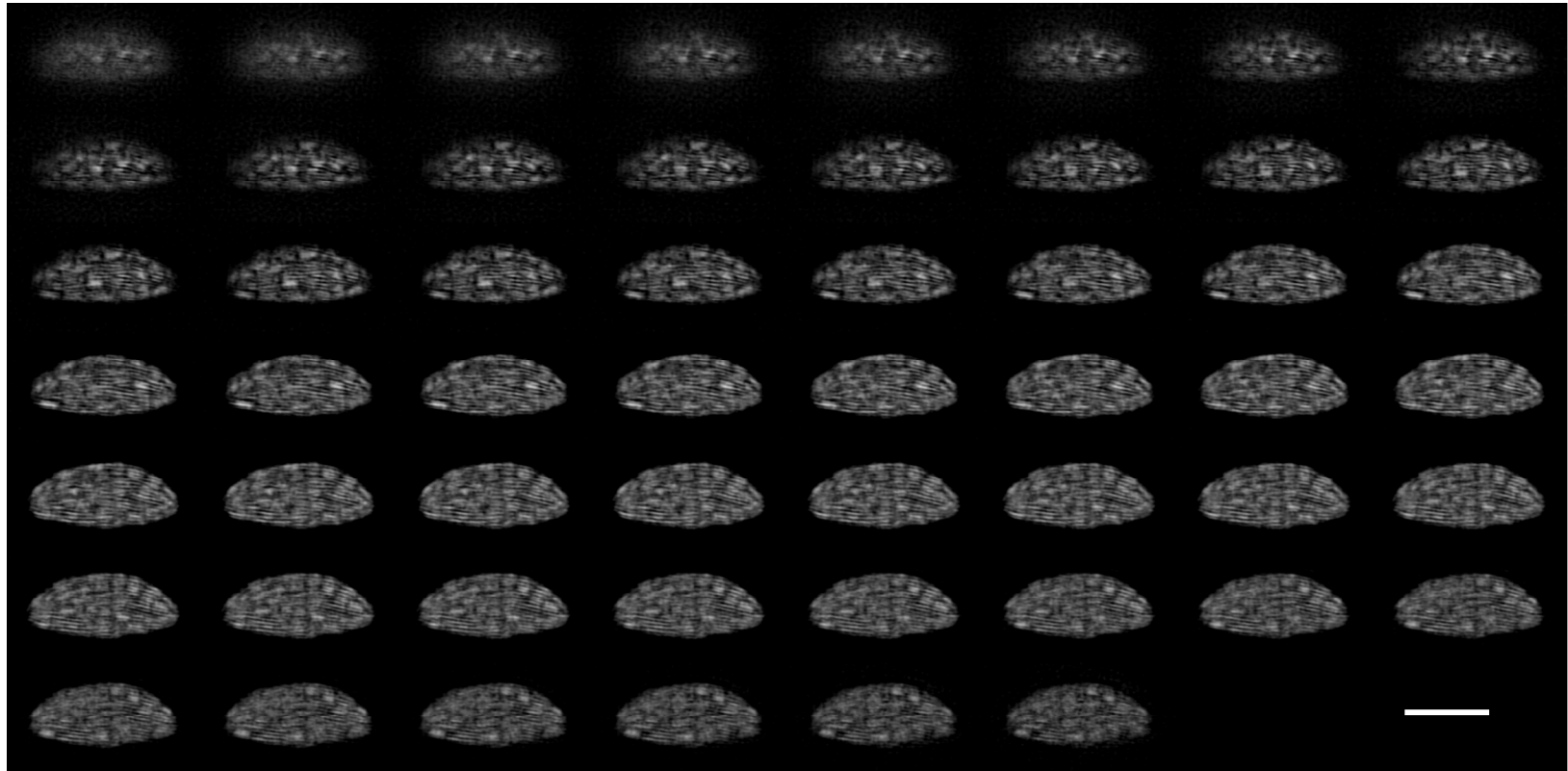


Figure S2. Optical sections of reconstructed 3D-SIM images of the side-view of the chloroplast isolated from *A. thaliana stn7 stn8* mutant leaves. The individual focal planes are shown in the order from top left to bottom right. Scale bar, 5 μm .

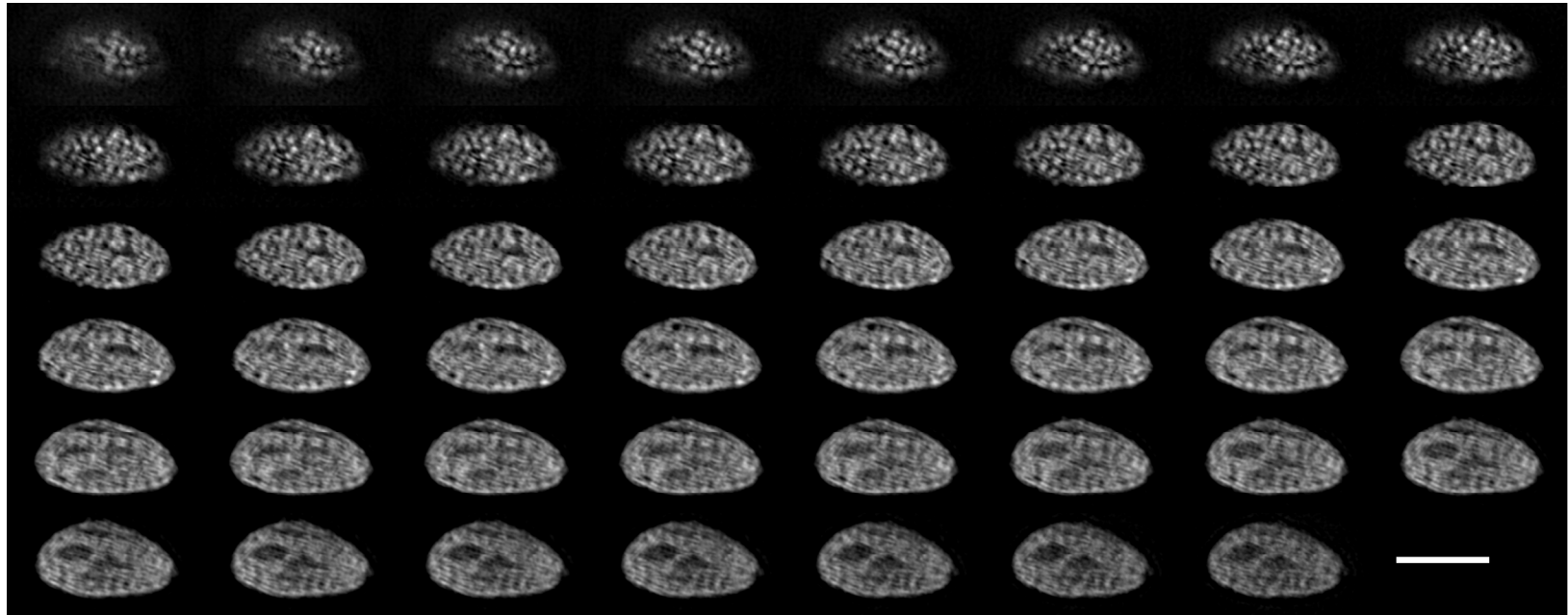


Figure S3. Optical sections of reconstructed 3D-SIM images of the side-view of the chloroplast isolated from *A. thaliana tap38* mutant leaves. The individual focal planes are shown in the order from top left to bottom right. Scale bar, 5 μm .

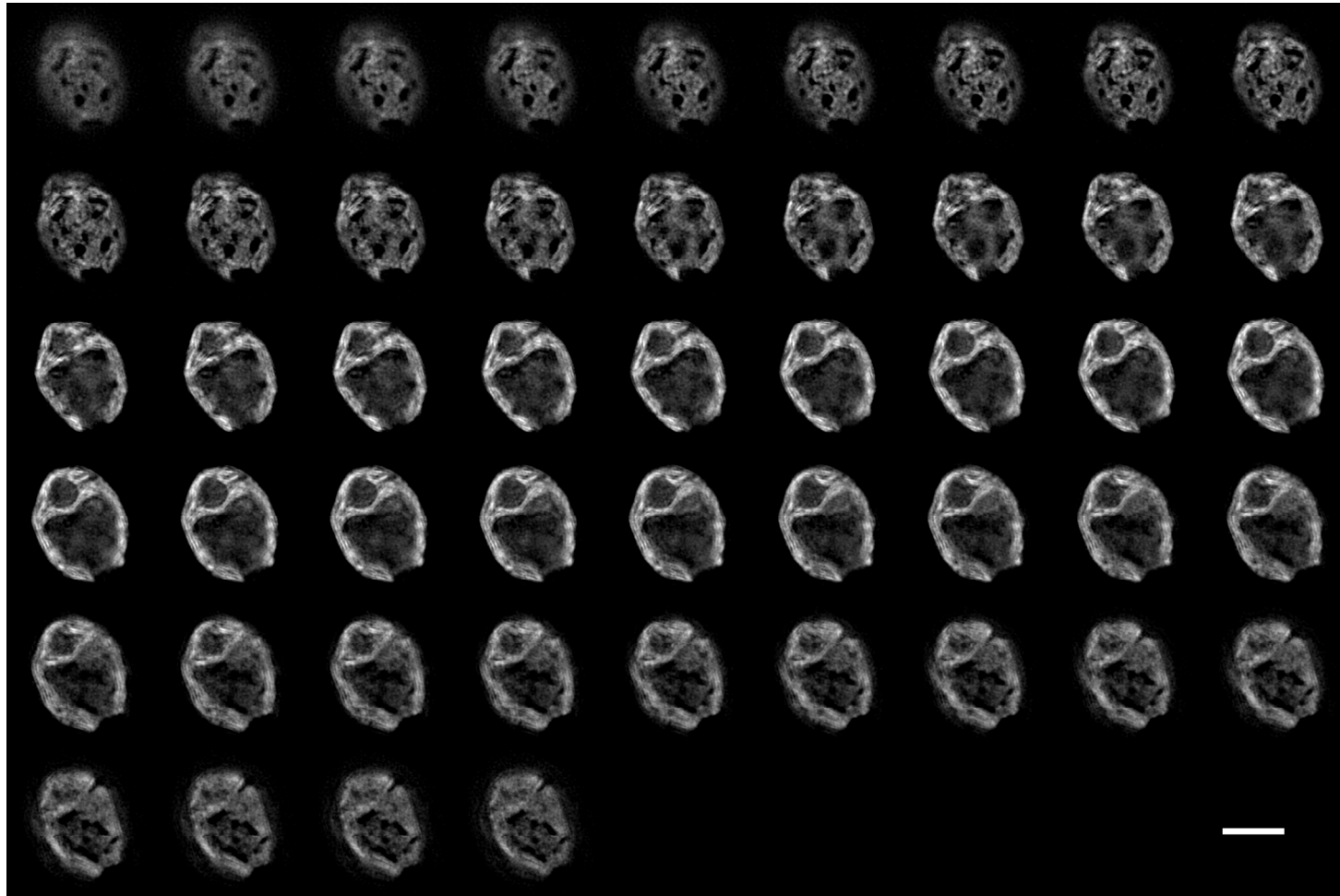


Figure S4. Optical sections of reconstructed 3D-SIM images of WT *C. reinhardtii* cell. The individual focal planes are shown in the order from top left to bottom right. Scale bar, 5 μm .

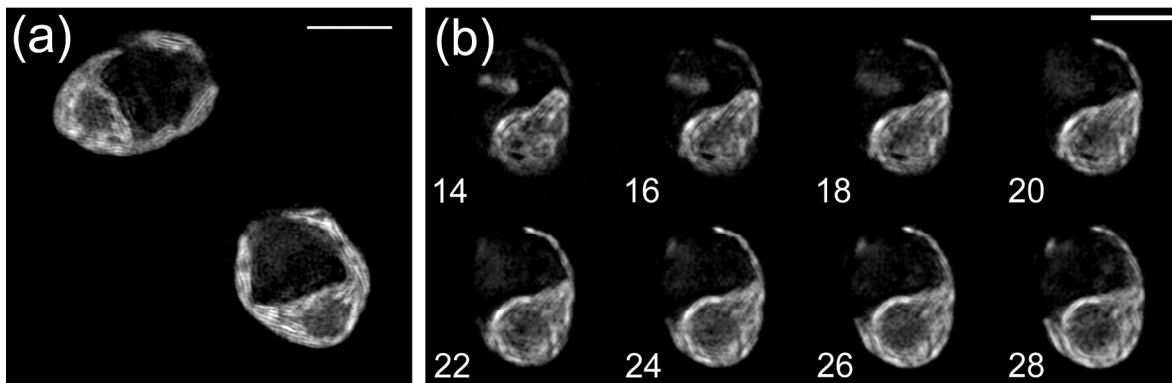


Figure S5. Additional reconstructed 3D-SIM images showing shrinkage of thylakoid membranes at the lobe region of *C. reinhardtii* chloroplasts under HL conditions for one day. (a) The cells grown under DL conditions ($\sim 5 \mu\text{mol photons m}^{-2} \text{s}^{-1}$), transferred to HL conditions ($\sim 350 \mu\text{mol photons m}^{-2} \text{s}^{-1}$) for one day, and then transferred to LL conditions for one day. The reconstructed 3D-SIM image shows the thylakoid membranes at the lobe region recovered. (b) Optical sections from the peripheral to central focal planes of phototrophically grown *C. reinhardtii npq4 lhcsr1* cell under DL and transferred to HL ($\sim 350 \mu\text{mol photons m}^{-2} \text{s}^{-1}$) for one day. The reconstructed 3D-SIM image shows the partial lobes of the thylakoid membranes. The numbers indicate the selected focal planes of the optical sections. Scale bars, 5 μm .